Modeling the effects of pilot injection strategies on combustion noise and soot emissions in a light-duty optical diesel engine

F. Perini[1], K. Zha[2], S. Busch[2], A. Warey[3], R. Peterson[3], R.D. Reitz[1]

[1]Engine Research Center, University of Wisconsin-Madison. Madison, WI, United States of America.

E-mail: perini@wisc.edu, reitz@engr.wisc.edu
Telephone: +(1) 608-263-2735

[2]Combustion Research Facility, Sandia National Laboratories. Livermore, CA, United States of America

E-mail: kzha@sandia.gov, sbusch@sandia.gov
Telephone: +(1) 925-294-1512

[3]Propulsion Systems Research Lab, General Motors. Warren, MI, United States of America

E-mail: alok.warey@gm.com, richard.peterson@gm.com
Telephone: +(1) 586-563-9703

Abstract. In this work a computational model of a single-cylinder optical research engine is used to study the effects of different pilot injection strategies on combustion noise and soot emissions in a light-duty optical diesel engine. The engine is equipped with an optical piston with a conventional re-entrant bowl, which retains all details of the corresponding metal piston.

The model is validated against measurements of combusting and non-combusting high-pressure diesel sprays in the Engine Combustion Network constant-volume chamber in terms of jet structure, ignition delay, lift-off length and soot volume fraction distributions, for chamber temperatures of 750 to 1200 K and O_2 concentrations of 15% to 21%. Mixture formation in the engine is validated against in-cylinder PLIF measurements from a single injection pulse for a low-load condition, and from a pilot injection.

A pilot injection sweep is performed for a moderate load operating condition with a single-pulse, near-TDC injection strategy operating conventional diesel combustion (CDC) as the baseline case. The engine fuel is a two-component Diesel Primary Reference Fuel comprised of 42% n-hexadecane and 58% heptamethylnonane, which features similar ignition chemistry and physical properties as a CN51 Diesel fuel. The sweep features several pilot-main energizing dwells from 80 to 1200 us, while pilot mass, load, and CA50 are held constant.

The study of the effects of the energizing dwell highlights two mechanisms responsible for the dynamics of soot formation and combustion noise in the engine. A first one involves the interactions between pilot and main jets: if the pilot injection is too close to the main, mixture forming from both creates a unique premixed combustion event, with stronger noise and a soot formation peak. A second one involves combustion thermodynamics: if the pilot has enough time to mix and burn completely before the main pulse starts, a dilution region is formed by the hot combustion products, so that the amount of premixed burn from the main is limited, and soot starts forming downstream as the jet impacts against the bowl rim.

1. Introduction

Pilot injections are a well-established strategy to control combustion noise from direct injection diesel engines [1,2]. In a pilot injection, a tiny amount of fuel is injected through a short pulse which precedes the main injection event. By the time the main pulse is injected, the pilot air-fuel mixture will have burned, increasing temperatures and active radical concentrations in the region of the charge that will mix with the fuel vapor from the major pulse. Consequently, ignition delay times will be reduced, reducing the amount of premixed fuel burn, and fostering a more sustained mixing-controlled mechanism that can reduce peak heat release rates, as well as peak temperatures. Modern common-rail fuel injection hardware is reported to allow up to eight injections per cycle [3], thus allowing broad optimization of these

strategies, by varying the amount of injected mass and the delay ('dwell') of each pilot injection pulse [4].

Many authors have focused on the effects of pilot injections on diesel combustion and emissions over the past years. In the works by Dürnholz et al. [2] and Badami et al. [5], the effectiveness of pilot injections in reducing combustion noise was assessed. Complex interactions between the pilot injection dwell and the resulting combustion noise were observed. At medium loads, the amount of noise reduction was seen to reduce, even leading to higher noise when the pilot injection was close to the main. High loads were instead seen to always provide lower noise when a pilot injection was employed. Ricaud and Lavoisier [6] studied multiple injection settings in a single-cylinder, small-bore engine equipped with a piezoelectric injector, varying dwell, injected quantity, rail pressure, EGR rate. They observed that the optimal dwell is correlated with the pilot fuel quantity, with small pilot amounts being preferred for intermediate dwells, and that peak heat release rates from the pilot and main injection are almost equal for noise-optimized injection configurations.

A number of previous studies have been conducted at the Sandia National Laboratories light-duty diesel engine facility with the aim of shedding light on the mechanisms of mixture formation, ignition, noise and late-cycle flow behaviour in presence of multiple injections and closely coupled pilot injections [7-13]. PLIF measurements were conducted to measure and understand the mixture preparation and pilot ignition limits for a wide range of operating conditions relevant to low-temperature combustion strategies [7-9]. The in-cylinder mixture preparation from a pilot injection highlighted that ignition delay times, which affect the 'minimum' amounts of dwell for a pilot-main injection strategy, should be extended significantly as more dilute, low-temperature conditions are being operated. Under these conditions, smaller pilot masses or higher injection pressures form still leaner mixtures, and further extend the ignition delay. Similarly, mixtures that are excessively rich, formed under more conventional diesel conditions, also result in longer ignition delays. Under these conditions, however, the leaner mixtures associated with smaller pilot masses or higher injection pressures will shorten the ignition delay. At a moderate load, conventional diesel combustion operating condition [10-13], it was observed that combustion noise can be drastically reduced by changing the dwell between the pilot and main injection energizing times by a fraction of a millisecond. In-cylinder pressure measurements and zero-dimensional simulations showed that two phenomena are essentially responsible for the significant noise reduction: the changing phasing of the pilot heat release event relative to the main heat release event, and suppression of the pilot AHRR by the main injection. However, a detailed understanding of how the pilot and main jet structures locally interact in the cylinder is not available yet.

The goal of this work is to close the gap by validating and assessing a multidimensional computational fluid dynamics (CFD) model of the SNL light-duty optical engine operated with the medium-load pilot-main injection strategy of [10], and analyzing the effects of energizing dwell time on combustion noise and soot emissions at this operating point. The computational model was built using FRESCO [14], a new, object-oriented parallel CFD simulation platform being developed at the University of Wisconsin. For code validation, non-reacting and reacting (sooting) spray simulations were performed against experimental data from the Engine Combustion Network in the Sandia constant-volume chamber, with meshes having the same resolution as the engine's computational mesh. Then, mixture preparation in the optical engine was validated against in-cylinder PLIF of mixture preparation. Finally, a combusting study considered a main CDC injection pulse, preceded by a pilot injection, 80 to 1200 μs earlier than the main injection event. Two effects were seen to contribute to combustion noise and soot emissions when varying pilot energizing dwells are employed. First, the physical interactions between pilot and main jets, when the pilot is too close to the main pulse, lead to a unique well-mixed charge which causes strong premixed combustion, noise and a soot peak. Second, if a dilution region is formed in case the pilot injection has enough time to mix and burn, the amount of premixed burn from the main is limited, and soot starts forming downstream as the jet impacts against the bowl rim.

2. Experimental setup

The engine experimental measurements were carried out at the Sandia National Laboratories light-duty optical engine facility [10]. The laboratory is equipped with a single-cylinder, modified version of the General Motors 1.9L light-duty diesel engine, provided with a Bowditch-style piston which can accommodate either a metal piston or an optical piston that retains full geometric details of the production piston, as well as optical access to the combustion chamber for allowing extensive measurements of local quantities in the squish region and in the piston bowl, as schematically represented in Figure 1.

The engine's intake runners are also provided with adjustable throttle plates for variable swirl generation, and different throttling strategies can be used to generate swirl ratios from about 1.5 up to about 5.5. A summary of the main engine characteristics is reported in Table 1. A blend of the diesel reference fuels (DPRF), n-hexadecane and heptamethylnonane, was used for both the reacting and non-reacting pilot injection experiments. This "DPRF58" blend was chosen to match the ignition delay and physical properties of conventional diesel fuel more closely than the Primary Reference Fuels (PRF) blend of n-heptane and isooctane used previously [7] for partially-premixed combustion research, and has been used in more recent studies [7-13]. Detailed thermo-physical properties for this fuel can be found in [9]. Thermodynamics, fuel properties and injection parameters for the operating conditions explored in the current paper are reported in Table 2.

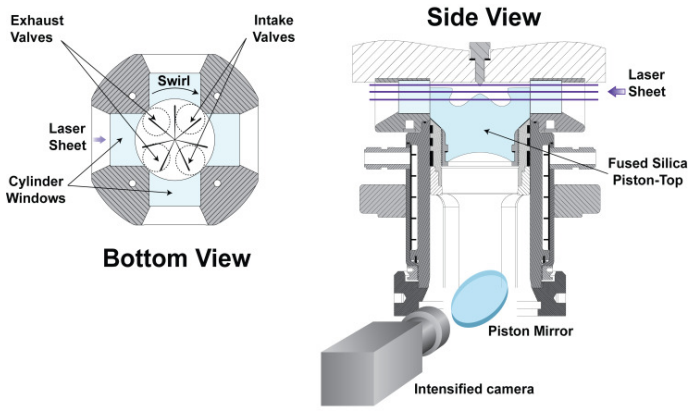

Fig. 1. Schematic representing the optical access engine setup, including the three laser sheet locations and camera viewing direction.

All of the experiments considered in this study were run at a fixed engine speed of 1500 rpm, and with variable intake conditions, but keeping an approximately constant intake pressure of 1.5 bar, mimicking a moderately boosted operating condition. The fuel injector used in this study is a solenoid multi-hole injector equipped with a pressure-balanced pilot valve. The injector features a mini-sac nozzle with seven holes, with diameter of 139 μm and an included angle of 149 degrees. Different pilot injection strategies were considered in this study. A single-pulse early injection, featuring 8.8mg of injected mass, and SOI = -23 degrees aTDC, typical of low-temperature combustion modes, was used for the model validation against in-cylinder local mixture fraction distributions, as this operating condition had been extensively tested in a number of previous studies [15,16]. Then, a single-pulse *pilot* injection sweep was considered. In the sweep, injected mass and injection pressures were varied, all pilots being always injected 15 degrees before top dead center (TDC), with a near-TDC density of 19.6 kg/m3, so as to limit the number of parameters affecting their ignitability to various local mixture conditions [7-9]. Both these sets featured measurements of local equivalence ratios having been taken in a non-reacting environment made up of pure nitrogen, and using a fuel tracer based planar laser-induced fluorescence technique (PLIF) that employs introduction in small quantities of a fluorescent tracer into the diesel surrogate mixture: 1-methylnaphtalene for the DPRF58 fuel, and toluene for the PRF25 mixture.

Table 1. Main engine and experimental setup specifications for the SNL light-duty optical engine

Engine specifications	
Bore x stroke [mm]	82.0 x 90.4
Unit displacement [cm^3]	477.2
Compression ratio	16.4 : 1
Squish height at TDC [mm]	0.88
Injector parameters	
Sac volume [mm^3]	0.23
Number of holes	7
Included angle [deg]	149
Nozzle diameter [mm]	0.14
Hole protrusion [mm]	0.3

Table 2. Main simulated operating conditions.

	Non reacting Spray A	Reacting Spray A	Non reacting PPC	Non reacting pilot	Reacting pilot
Intake charge [mol fr.]	100% N_2	15.0% O_2 75.2% N_2 6.2% CO_2 3.6% H_2O	100% N_2		19.7% O_2 78.7% N_2 1.6% CO_2
Intake pressure [bar]	59.5	49.3,53.1, 56.3,59.1, 66.2,73.4,79.4	1.5		
Intake temperature [K]	900	750,800, 850,900, 1000,1100,1200	300	303 to 403	353
Engine speed [rev/min]	---	---	1500		
Swirl ratio (Ricardo) [-]	---	---	2.2		
Injection properties					
Injected fuel mass [mg]	3.6	13.77	8.8	1.0, 2.0, 3.0, 4.0	1.5+24.5
Injection pressure [bar]	1500	1500	860	500, 860	800
Start of pilot injection [deg]	---	---	---	-15.0	-13.3, -5.2, -3.2
Start of main injection [deg]	0.0	0.0	-23.3	---	-2.5
Fuel properties					
Composition [mole fractions]	100% $C_{12}H_{26}$		25% iC_8H_{18}	42% $nC_{16}H_{34}$	
			75% nC_7H_{16}	58% iso-$C_{16}H_{34}$	
Fluorescent tracer [mass fr.]	--	--	0.5% C_7H_8	0.5% 1-$C_{11}H_{10}$	
Equiv. Cetane Number [-]	--	--	47.0	50.7	

3. Model validation

Modeling of pilot injection phenomena is a challenging task for computational simulations. The fuel injection process is transient, the injector needle never reaches its maximum lift, and transient internal nozzle hydrodynamics amplify non-deterministic phenomena, such as non-negligible presence of fuel dribble, and non-homogeneous nozzle-by-nozzle behavior. These phenomena lead to macro-scale effects, such as a shift in the pilot injection's ignitability properties from what is observed with well-mixed, homogeneous reactor calculations [8]. For these reasons, to build a computational model capable of reproducing pilot injection events, it was necessary to validate it on more elementary steps first, in order to avoid any further sources of uncertainty.

All simulations were performed using FRESCO [14], a new, object-oriented parallel platform for multidimensional engine simulations being developed at the University of Wisconsin-Madison. The code implements an unstructured, parallel volume-of-fluid solver for the Navier Stokes equations, with automatic domain decomposition for variable-topology meshes. The spray models implement advanced parallel algorithms for breakup, collision, vaporization and near-nozzle flow dynamics [17]. Combustion chemistry is handled by a sparse analytical Jacobian chemistry solver and high-dimensional-clustering based chemistry dimensionality reduction [18,19]. A list of the sub-models employed for the current study is reported in Table 3.

The computational model, capable of modeling pilot-main injection cases, was defined after all sub-models for spray, combustion and soot formation were validated against reference experimental set ups. All spray model constants were not changed from a previous genetic-algorithm-based optimization study, which highlighted an optimal set of constants for modeling Spray A simulations [17]. In particular, for the Kelvin-Helmholtz breakup model, a timescale constant $B_1 = 40.6$ and a wavelength constant $C_{\Lambda,KH} = 0.61$, in combination with a Levich breakup length multiplier $L = 1.94$, were used. Rayleigh-Taylor breakup constants, which define the drop size distribution after catastrophic collapse of the drops, were $C_{\tau,RT} = 0.10$ for the timescale, and $C_{\Lambda,RT} = 0.05$ for the wavelength. The sub-grid scale near nozzle gas jet model employed an assumed Stokes number St=0.15, an air entrainment constant Kentr = 0.85, and a maximum smoothing factor $\gamma_{max} = 0.9$. It should be noted that the spray model configuration was run

in simulations employing a generalized RNG k-epsilon turbulence model [20], which includes an anisotropy-based dimensionality correction factor. The GRNG turbulence model allows the same model to be shared between spray jet simulations and diesel engine simulations, where standard k-epsilon models do not perform acceptably well because of the combination of compression and swirling components in the stress tensor [37]. Finally, because the fuel surrogates used in the experiments used well-defined measured compounds, the validation of spray, combustion and soot formation models could be done by modeling the fuel's physical and chemical properties, and their effect on injection, atomization, vaporization, mixing and ignition. Also, for consistency among the different experiments being model, similar mesh resolution as the one used in the engine model was used.

Table 3. Main sub-models employed in FRESCO for the present study.

Phenomenon	**Sub-model**
Spray breakup	Hybrid KH-RT instability, Beale and Reitz [21]
SGS near-nozzle flow	Unsteady gas-jet model with implicit momentum coupling, Perini and Reitz [17]
Spray angle	Reitz and Bracco [22]
Drop drag	Analytical with Mach number effects [17]
Droplet collision	Deterministic impact with extended outcomes, [23], dynamic ROI (radius-of-influence), [17]
Evaporation	Discrete multi-component, Torres [24]
Turbulence	Generalized RNG k- ε, Wang and Reitz [20]
Chemistry solver	Sparse Analytical Jacobian (*SpeedCHEM*), Perini et al. [18]
Chemistry grouping	High-Dimensional Clustering, Perini et al. [19]
Piston compressibility	Static, Perini et al. [16]

3.1 Non-reacting Spray A

The first validation featured the spray and fuel jet structure, and was performed by modeling the Engine Combustion Network non-reacting Spray A experiments, which use n-dodecane fuel, T=900K ambient temperature, and 0% oxygen [25]. In order to test grid dependency of the spray model, two grids were generated, whose details are reported in Table 4, and as shown in Figure 2 for the refined mesh. The mesh structures feature a jet-shaped inner core, with a geometric cell height progression that has a minimum near the nozzle, and increases along the jet axis. The square-shaped inner core is then extended outward using an o–grid structure until the limits of the combustion vessel, where much larger cell sizes are used. Downstream of the nozzle, the inner core extends conically with a semi-cone angle of 5.5 degrees. In this way, it was possible to use a full three-dimensional mesh representation of the ECN vessel, while keeping adequate resolution in the jet region.

A first, 'coarse' spray grid has an average near-nozzle cell size of 1.0 mm which mimics the resolution adopted in the engine simulation, and a total of about 19k cells. The 'refined' mesh has a near-nozzle size of 0.25 mm, and about 311k cells total.

Table 4. Mesh details for the Spray A calculations

Mesh	**Cells**	**Nodes**	**Cell Δx at nozzle**	**Wall time (8 cpu)**
Refined	310944	318800	0.25 mm	3.02 h
Coarse	19053	20280	1.00 mm	0.51 h

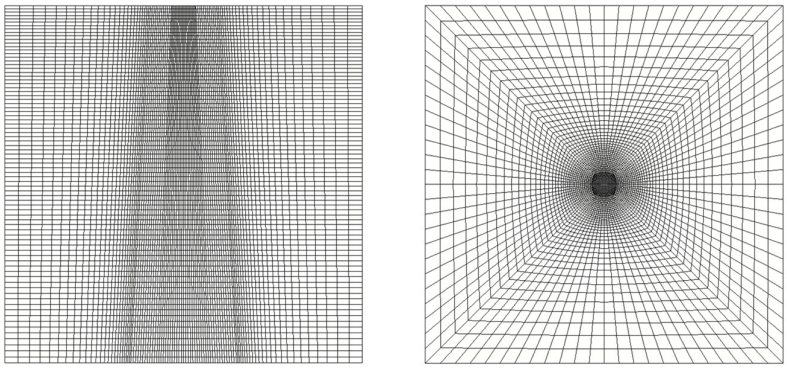

Fig. 2. Vertical (left) and horizontal (right) cut-planes representing the spray-oriented structure in the 'refined' mesh used for modelling the ECN spray experiments.

Vapor and liquid penetration results are reported in Figure 3. The liquid penetration predictions were evaluated computing the downstream location where the cumulative liquid mass reached 90% of the total instantaneous liquid fuel in the chamber; the vapor penetration was computed as the farthest cell centroid location where a fuel volume fraction of at least 10 ppm was present. The simulations showed some grid dependency of the liquid penetration predictions, with the refined mesh exhibiting the shorter penetration. However, considering the uncertainties also associated with the experimental process, both predicted cases appear acceptable. Both cases show well converged predictions of vapor penetration in the chamber, the coarse mesh just only slightly under predicting vapor penetration around t = 1 ms. Overall, both cases exhibit very good agreement with the experimental vapor penetration curve.

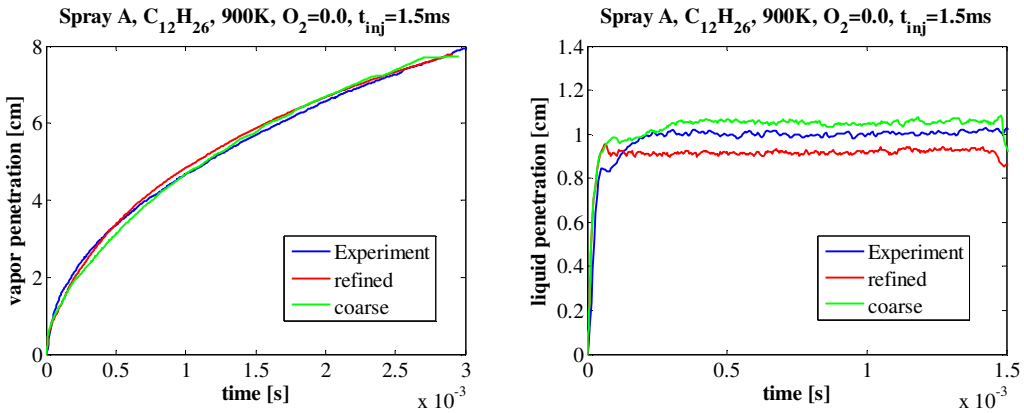

Fig. 3. Non-reacting Spray A validation: predicted vapor (left) and liquid (right) penetration versus the experimental measurements of [25].

The same cases were also compared to quasi-steady-state fuel mixture fraction distributions in the chamber, along the injection axis as well as radially, at select downstream locations, as reported in Figure 4. Both simulations capture radial mixture fraction distributions very well at the most downstream locations, while some discrepancies emerged closer to the injector. In the near-nozzle region, the refined mesh showed some overestimation of the fuel mixture fraction close to the centerline, which however dissipated later on, and without affecting the global radial jet spread angle, which was predicted correctly. However, this does not seem to negatively affect the bulk jet structure far from the liquid region, and sufficient accuracy is achieved even with a relatively coarse mesh resolution of about 1 mm.

3.2 Reacting Spray A

The same simulation was used to validate reactive and sooting Spray A experiments, employing the same n-dodecane fuel and similar high-pressure, high-temperature chamber conditions from [26]. In the

reacting simulations, a reduced n-dodecane reaction mechanism previously validated against soot formation predictions was used [27]. The soot formation rate is modeled according to the two-step approach of Hessel et al., [28], using the single-equation Hiroyasu model [29] for the soot formation term, acetylene as the soot-forming species and the Nagle and Strickland-Constable model [30] for the O2-based soot oxidation mexhanism:

$$\begin{cases} \dfrac{d\rho_s}{dt} = \dfrac{d\rho_{s,f}}{dt} - \dfrac{d\rho_{s,o}}{dt}; \\ \dfrac{d\rho_{s,f}}{dt} = A_{s,f}\rho_{C_2H_2}p^{0.5}e^{-E/T}; \\ \dfrac{d\rho_{s,o}}{dt} = \dfrac{6W_C}{\rho_C D_s}\rho_s f_{NSC}\left(T, p_{O_2}\right); \end{cases}$$

where subscript *s* stands for soot, *f* for formation, *o* for oxidation, E = 12.5 kcal/mol is the soot formation activation energy, W_C=12.001 g/mol the carbon's molecular weight, ρ_C = 2g/cm^3 the solid carbon density, D_s the assumed soot particle diameter. In the Nagle and Strickland-Constable function, f_{NSC}, the updated rate coefficients by Vishwanatan and Reitz [31] were employed.
The effects of mesh resolution on the predicted flame structure is reported in Figure 5. Both meshes predict similar flame lift-off length, as well as flame shapes, and similar peak values for

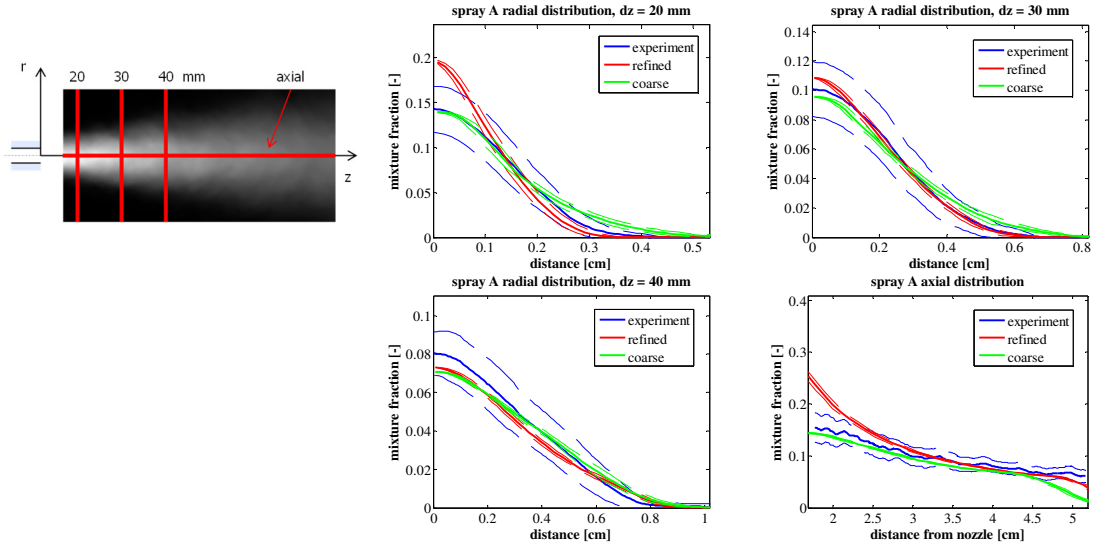

Fig. 4. Non-reacting Spray A validation: predicted mixture fraction distributions along the injector axis and at different radial locations versus measured data [25].

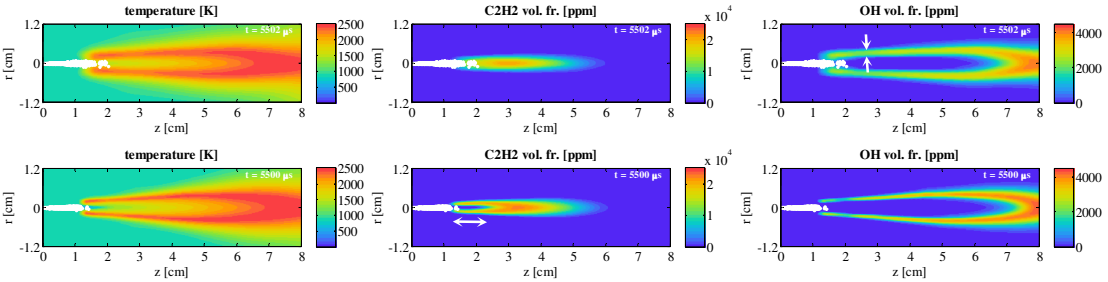

Fig. 5. Effect of mesh resolution on predicted reacting Spray A features: from the left, temperature, C2H2 mole fraction, OH mole fraction. (top) coarse mesh, (bottom) refined mesh.

both temperature and radical concentrations are seen. Differences due to the different grid resolution are noticed in terms of the reactive layer thickness, which is noticeably thinner for the refined mesh case, and inner flame core at the interface between liquid and gas-phase, 1.5 to 2.0 mm downstream of the injector, where the coarse mesh cannot capture the acetylene formation region and predicts an almost homogeneous concentration.

The flame lift-off length for 15% O_2, 22.8 kg/m^3 reactive Spray A condition was analyzed according to the ECN guidelines by Skeen et al. [32], as reported in Figure 6, using the coarse mesh whose resolution is similar to that of the present engine simulations. The average OH radical concentrations versus axial distance from the nozzle is computed, and the instantaneous lift-off length is identified as the location at which OH concentration reaches 50% of the maximum concentration, during the initial ramp-up region, i.e., before reaching the near-steady downstream plateau. A vessel temperature sweep was run with ambient temperatures ranging from 750K to 1200K and compared with the experimental measurements – as well as computational results from other Institutions – reported by Skeen et al. [33]. The comparison is reported in Figure 7 together with corresponding ignition delay computations, which show the time at which the maximum temperature rise rate for the cell with maximum temperature in the chamber occurs.

The FRESCO calculations are seen to capture the temperature dependency of lift-off length and ignition delay time reasonably well, with the absolute values for lift-off being in better agreement especially for the lowest temperatures, despite the slightly over-predicted ignition delays. At the higher temperatures, the model tends to predict a lower lift-off length, which is in line with the amount of near-liquid-jet mixing suffered by the coarse mesh due to the lesser grid resolution.

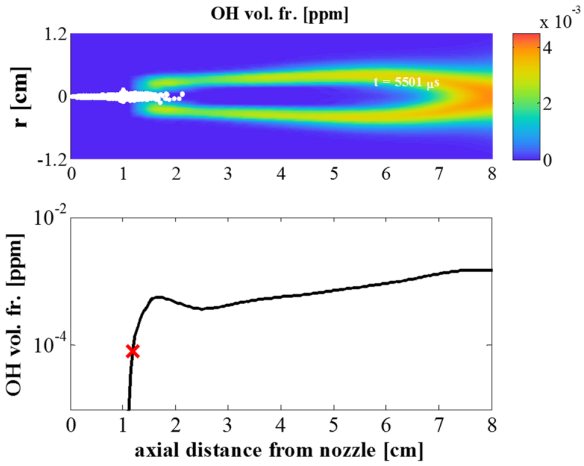

Fig. 6. Lift-off length calculation method, adapted from the experimental methodology of [32].

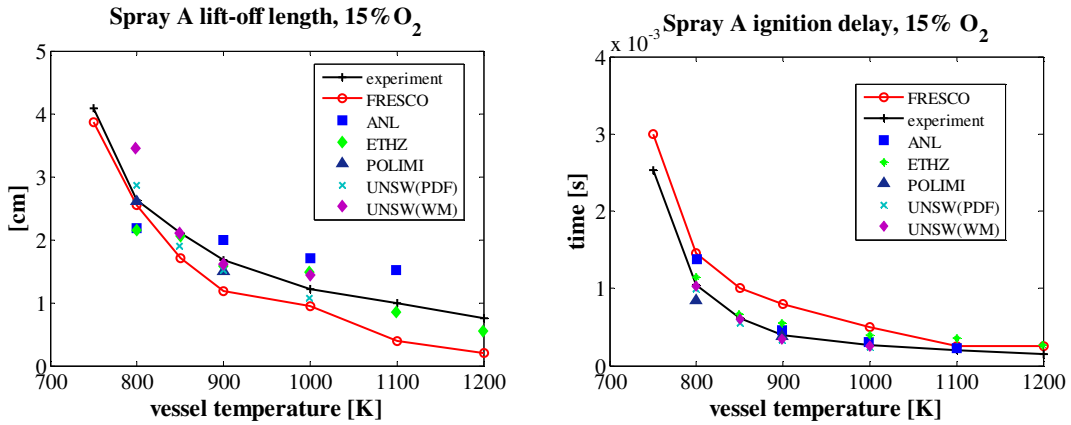

Fig. 7. Comparison between measured and predicted Spray A lift-off length (left) and ignition delay time (right) for an n-dodecane, 15% O2, 900K Spray A case; Dots represent computations from various institutions, reported in [33].

The soot formation and oxidation model has been well established over the past decades, even though it lacks soot oxidation via OH [31]. Hence, the soot formation pre-exponential factor was used as a unique calibration constant. A value of $A_{s,f}$ = 2.4e3 was determined as the 'optimal' value for the current configuration, as it was able to match quasi-steady-state soot mass in the Spray A vessel for the baseline 900K, 15%O2, 22.8 kg/m3 case, which has similar near-TDC oxygen concentration and ambient density to the engine cases.

The soot formation constant calibration is reported in Figure 8, and was exercised against local measurements of soot-driven optical thickness in the Spray A chamber, as reported in Figure 9. While the two quantities are not directly comparable, the sooty structure of the flame appears well captured: the peak soot concentrations form in the central part of the jet, as from [34], and stretch along the injection axis as the jet structure reaches quasi-steady-state conditions.

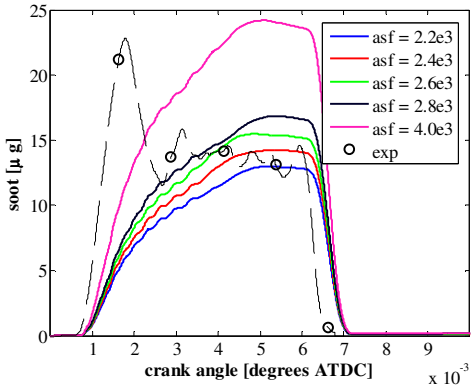

Fig. 8. Effect of Hiroyasu's soot formation model pre-exponential factor against measured Spray A soot mass, 15% O2, 900K, 22.8kg/m3, c12h26.

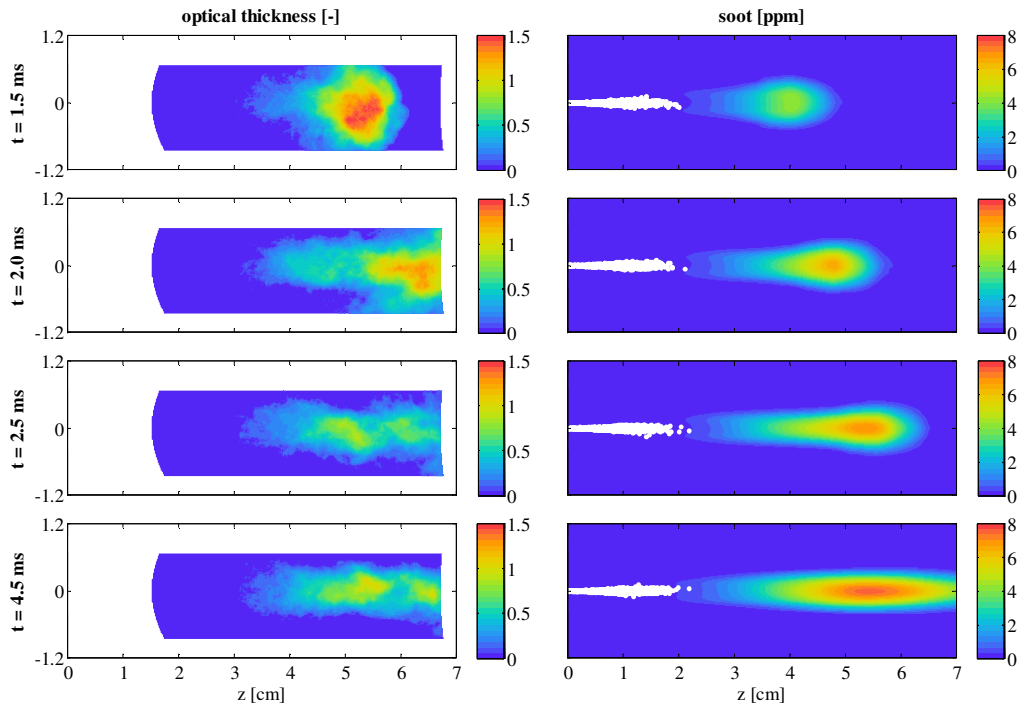

Fig. 9. Time evolution of soot distribution: measured (left, [35]) optical intensity and predicted (right) soot volume fractions for an n-dodecane, 15% O2, 900K Spray A case.

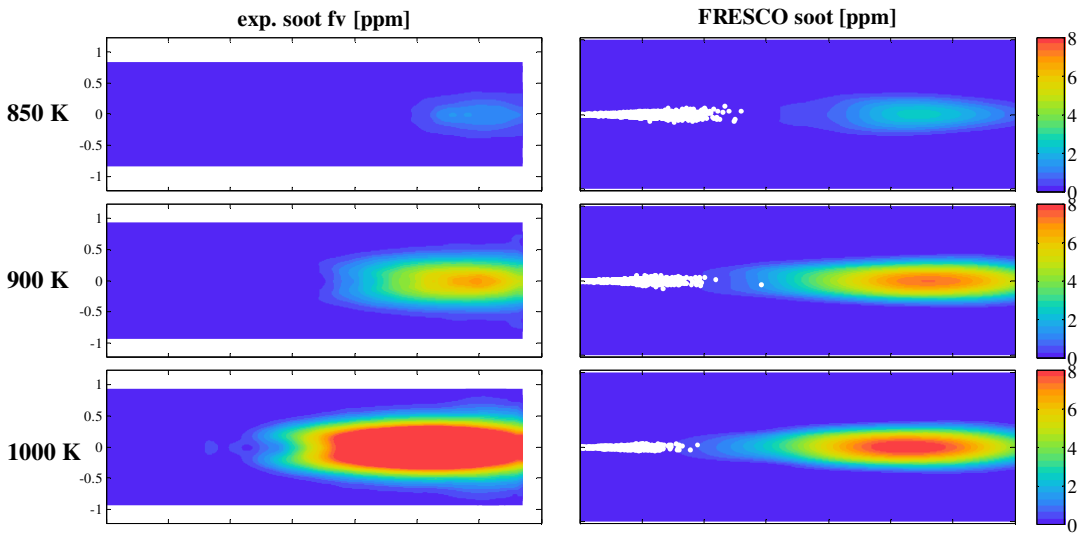

Fig. 10. Soot temperature dependency. (Left) Measured ([33]) and (right) predicted soot volume fractions for an n-dodecane, 15% O2, 22.8kg/m^3 Spray A case, with ambient temperature of 850K, 900K and 1000K.

The effect of ambient temperature on flame soot density is reported in Figure 10, with ensemble-averaged soot volume fraction data determined from experimental measurement of particle sizes in the ECN vessel [36]. Simulated soot volume fraction was computed by assuming a constant soot 'molecular weight' corresponding to an average agglomerate size with a particle mass of 10^{-14} [36], which corresponds to an average soot 'molecular weight' of W_{soot} = 6.02e3 g/mol, corresponding to a composition of an average soot agglomerate of C_{502}.

The comparison shows that the simple soot model captures the temperature trend, both in terms of peak soot concentration and its downstream location, as well as overall soot distribution. There is a slight underprediction of soot volume fraction at the 1000K ambient temperature.

3.3 Mixture formation in a light-duty engine

Model validation was conducted using experimental measurements of local spatial distributions of in-cylinder mixture equivalence ratio from a single injection pulse characterizing a partially-premixed combustion (PPC) operating condition [15,16], as well as for a pilot injection pulse [7,8] in the 1.9L engine. The operating conditions are reported in Table 2, while a full description of the experimental setup and measurement procedure can be found in the aforementioned references. The computational mesh reported in Figure 11 represents one azimuthal sector of one seventh of the combustion chamber, and has an average cell width of 0.7 mm [16], featuring 92850 total cells at BDC. The number of near-TDC cell layers was set to 10. Injection rate profiles for the different injection pressures and injected mass values were measured using an 8.8mg single injection pulse, and directly employed for the scaled from measured rates , using the procedure reported in [9].

3.3.1 Low-load, single-pulse PPC injection

A comparison between predicted and measured in-cylinder mixture fraction distributions from a single-pulse PPC injection event is reported in Figures 12-13. Select crank angles of 15, 10 and 5 degrees before TDC are reported, corresponding to approximately 3.15, 8.15 and 13.15 degrees after the end of injection. For the sake of brevity, only two engine swirl ratio configurations (bench Rs=2.2 and 3.5), out of the four experimentally tested, are reported here.

The model appears to capture reasonably well both the spray jet penetration into the squish region and at the bowl rim, as well as the peak equivalence ratios at any of the observation planes. In particular, at early crank angles, the near-nozzle jet part is predicted to have larger equivalence ratios, due to the Coanda effect which pushes the near-head jet region upward. Also, jet distortion due to the swirling

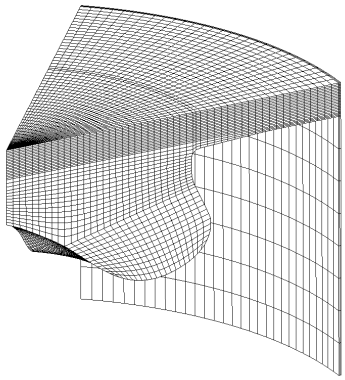

Fig. 11. Computational mesh employed for modeling the 1.9L light-duty, optical single-cylinder engine.

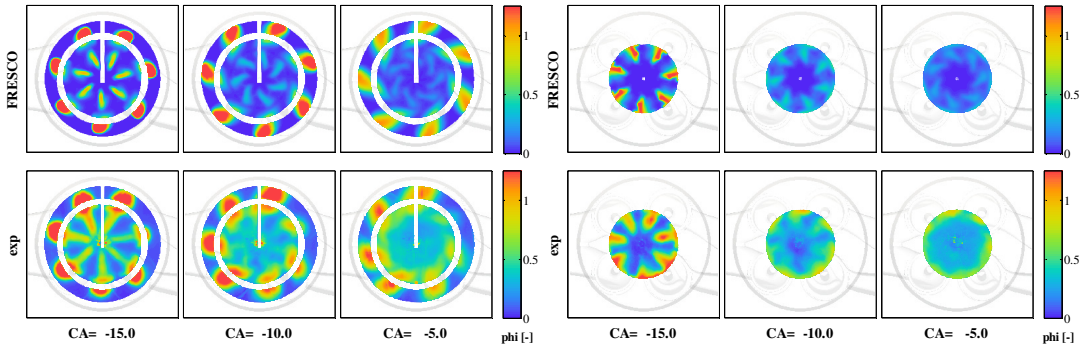

Fig. 12. Predicted vs. measured [15] mixture formation from a PPC injection pulse, Rs=2.2, p_{inj}=860 bar. (left) squish plane; (right) bowl rim plane.

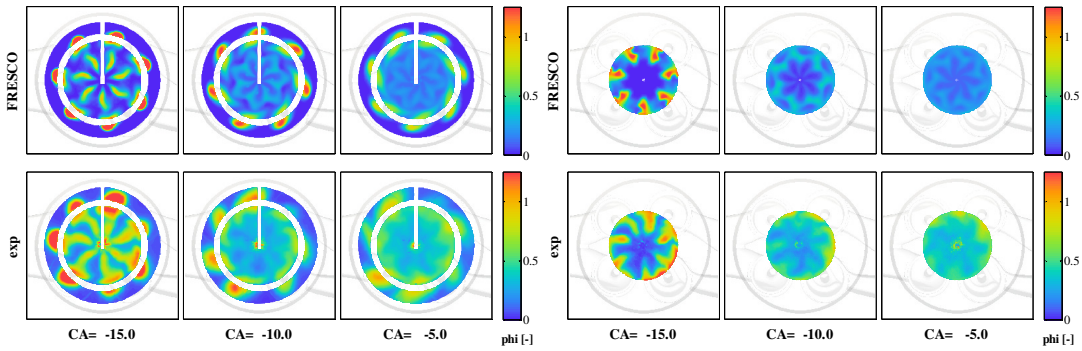

Fig. 13. Predicted vs. measured [15] mixture formation from a PPC injection pulse, Rs=3.5, p_{inj}=860 bar. (left) squish plane; (right) bowl rim plane.

motion is appropriately modeled. The jet tip penetration into the squish region is correctly predicted to reach the liner by the final crank angle, and to have a near-stoichiometric peak equivalence ratio in this area, which is surrounded by a significant amount of overly lean mixture.

As for the jet structure impacting the bowl rim and monitored at the bowl rim height plane, the simulations at both swirl ratio values capture an initial, jet-axis-centered compact structure having peak equivalence ratios of about 1.25, which mixes due to swirl into a much more homogeneous, less coherent charge having lean equivalence ratios in the 0.4-0.5 range.

3.3.2 Medium-load pilot injection.

A similar analysis was conducted for a single-pulse, pilot injection starting 15 degrees before TDC and injecting 1 to 4 mg of DPRF58 fuel into a near-TDC 19.6 kg/m3 density environment, corresponding to a medium-load operating condition. The simulations were compared with the experiments of [7,8]. Figures 14 and 15 report highlights of in-cylinder equivalence ratio measurements for injected masses of 2 and 4 mg at different crank angles, while Figures 16 and 17 report the effects of an injection mass sweep at 4 degrees before TDC, from an observed located below the piston.

For all injected mass values and measured crank angles, the experimental imagery exhibits significant jet-to-jet variation which is of course not captured by the present sector model. In particular, the jets forming from three of the nozzles exhibit much larger peak equivalence ratios, as well as somewhat deeper penetration downstream along the injection axis, which leads to an earlier impact against the piston bowl rim. The other jets exhibit a relatively similar behavior, which compares reasonably well with the simulation. For a 2mg injected mass (Fig. 14), peak equivalence ratios of about 0.5 are seen in the squish plane. The penetration is noticeably deviated by the swirl flow, and the pilot jet reaches the squish near TDC. Looking at the deeper bowl rim plane, higher near-stoichiometric equivalence ratios are seen at 8 deg aTDC, immediately after the end of injection. This rich mixture quickly mixes into an overly lean one, together with a loss of coherence of the pilot jet. This behavior is clearly seen both in the experiment and simulation.

In case of an injected mass of 4mg – i.e., at the upper size limits for a pilot injection in the light-duty engine – the mixture formation dynamics appear similar, but 'enhanced' by richer equivalence ratios.

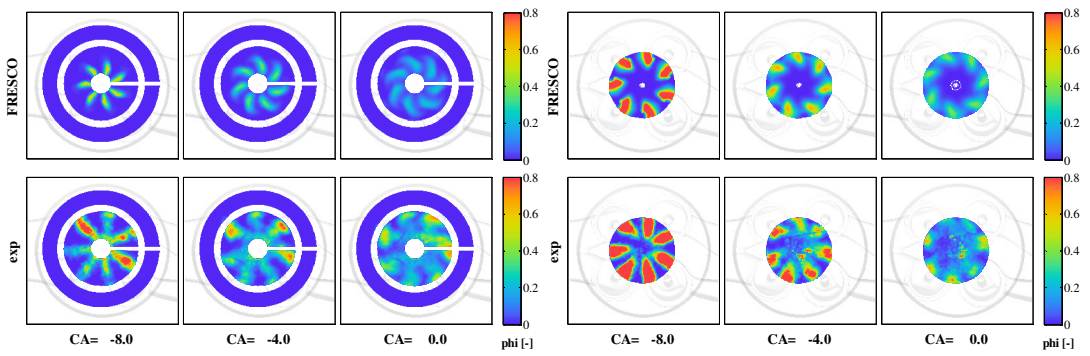

Fig. 14. Predicted vs. measured [7] mixture formation from a pilot injection, Rs=2.2, p_{inj}=860 bar, T_{TDC} = 930K, m_{inj} = 2mg. (left) squish plane; (right) bowl rim plane.

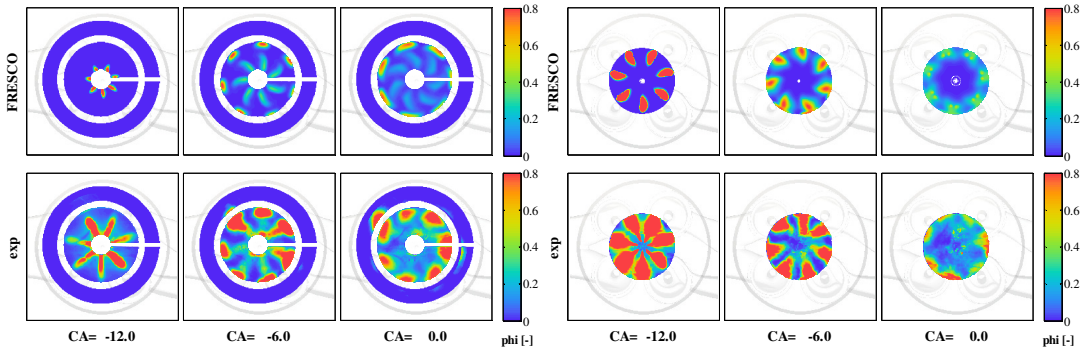

Fig. 15. Predicted vs. measured [7] mixture formation from a pilot injection, Rs=2.2, p_{inj}=860 bar, T_{TDC} = 930K, m_{inj} = 4mg. (left) squish plane; (right) bowl rim plane.

In the bowl rim plane, similar behavior happens as for the lower injected mass: a rich well-formed jet progressively mixing towards equivalence ratios which are slightly higher than for the 2mg injection, but still steadily lean. The injection has instead higher penetration into the squish region, which is reached as early as 6 degrees before TDC, where a bulk mixture pocket forming in the upper region surrounding the bowl rim is seen. This is the region typically targeted by the main injection pulse.

The differences in jet structure with varying pilot duration are reported in Figures 16 (squish plane) and 17 (rim plane) at 4 degrees before TDC. In the squish plane, a steady increase in penetration is seen, without changing the distorted structure impressed by the swirl in the central region, even for the 3 and 4 mg injections, where the jet tip hits against the rim, forming a local fuel vapor pocket. The same steady increase in penetration is also seen in the bowl rim plane, both of the leading and the trailing regions of the jet slice being intersected at this plane. In terms of equivalence ratio, similar peak values are seen also retaining the original well-formed jet structure.

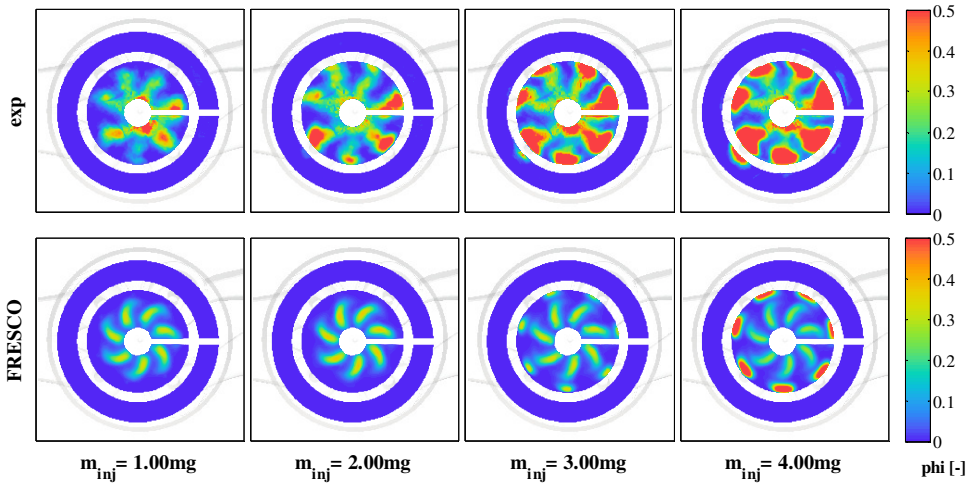

Fig. 16. Effect of injected pilot mass on squish equivalence ratio distribution at -4 deg aTDC: (top) experiments [7] vs. (bottom) simulation.

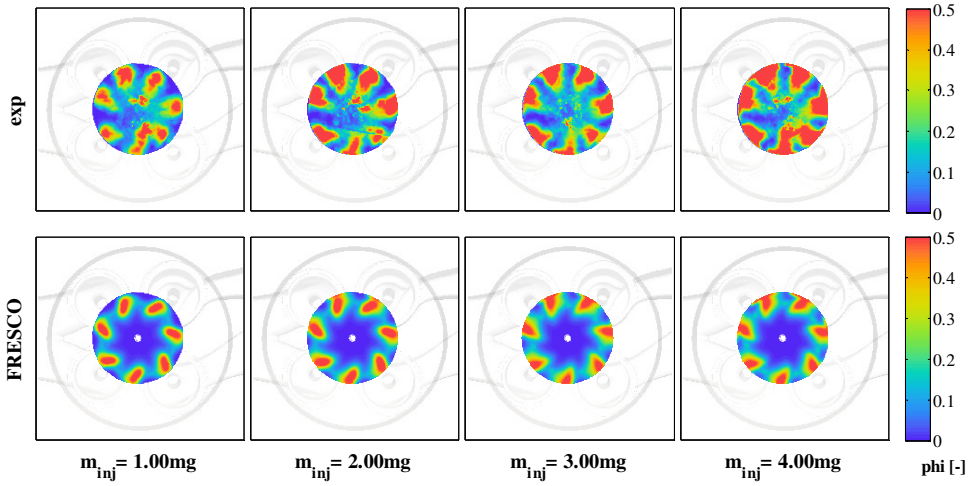

Fig. 17. Effect of injected pilot mass on equivalence ratio distribution at the bowl rim plane, -4 deg aTDC: (top) experiments [7] vs. (bottom) simulation.

4. Results

A pilot injection sweep simulation study was performed against the corresponding set of pilot-main injection experiments [10] (Table 2). The engine was fuelled using the same DPRF58 mixture as for the non-reacting pilot mixture preparation study. The sweep featured different pilot-main energizing dwells, from 80 to 1200 microseconds, while pilot mass, $IMEP_g$ and CA50 were held constant. The resulting injection profiles are reported in Figure 18 a).

Combustion development and noise.
Predicted and measured ensemble-averaged in-cylinder pressure traces are reported in Figure 18 b). When the pilot injection is far enough from the main injection pulse, it causes a step-wise increase in in-cylinder pressure, representative of the pilot burning pre-mixed, followed by a motoring-like pressure plateau until the main injection happens. The more favorable thermodynamic conditions and the enhanced mixing propensity of the now-partially-ignited mixture smooth the premixed combustion part following the main injection event.

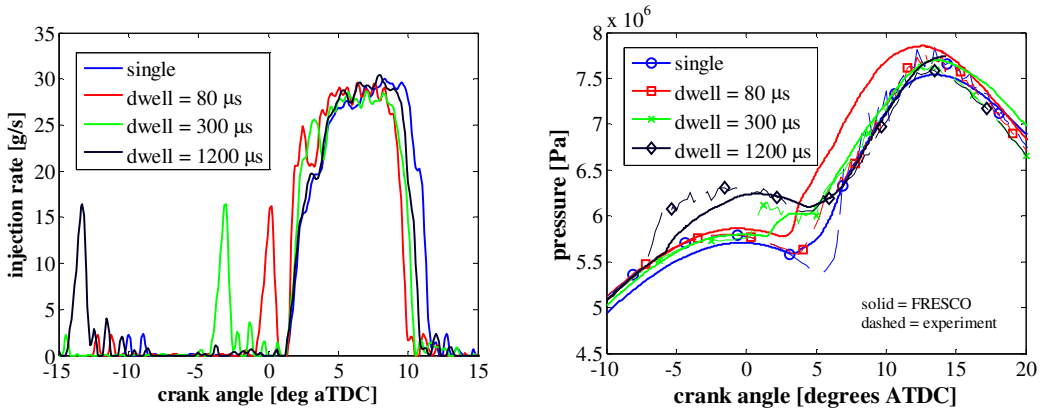

Fig. 18. Pilot injection study: Injection rate profiles (left) and predicted vs. measured in-cylinder pressure (right) for single injection, and pilot-main injection strategies with dwell time 80, 300, 1200 µs.

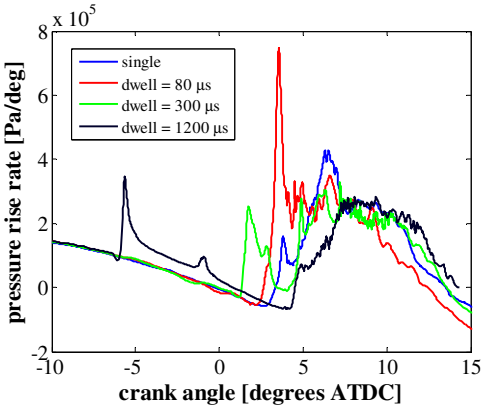

Fig. 19. Predicted in-cylinder pressure rise rates (in Pascal per crank angle degree) for single injection, and pilot-main injection strategies with dwell time 80, 300, 1200 µs.

The in-cylinder spray and flame structure is reported in Figure 20 at some relevant crank angles. For a single injection pulse, a traditional [34] flame development is seen: at 5 degrees aTDC, i.e., soon after the injection starts, a premixed burn of the initially injected mixture causes abrupt heat release and a high peak pressure rise rate; later, combustion is stabilized by a mixing-controlled mechanism as the injection and the jet splitting at the bowl rim, push burnt mixture azimuthally, while newly formed fuel vapor is being mixed with the remaining fresh charge.

Simulated pilot combustion takes place within the piston bowl – in agreement with the experimental observations of [11]. When a pilot injection is added too close to the main injection event, such as for an 80 μs dwell, the premixed ignition part is worsened, singe the premixed heat release involves both pilot and main fuel, causing higher peak pressure rise rate. As the in-cylinder images point out, at 2.5 degrees aTDC, when the main injection starts, the pilot injection still has significant momentum, causing faster penetration of the main injection towards the rim. By 5 degrees aTDC, the pilot mixture's premixed burn almost simultaneously overlaps with the fully formed main injection, causing a unique strong premixed ignition.

A pilot injection dwell of 300 μs does instead a much better job at smoothing the peak premixed heat release curve. Figure 20 well shows that, by the time the main injection reaches the rim (at 5 degrees aTDC), the pilot injection has already completely burnt, and has been partially rotated by the swirl. Hence, the main injection development benefits from a shorter ignition delay due to the chamber's higher temperature and pressure, avoiding the risk to add up to another well-mixed and already reactive charge.

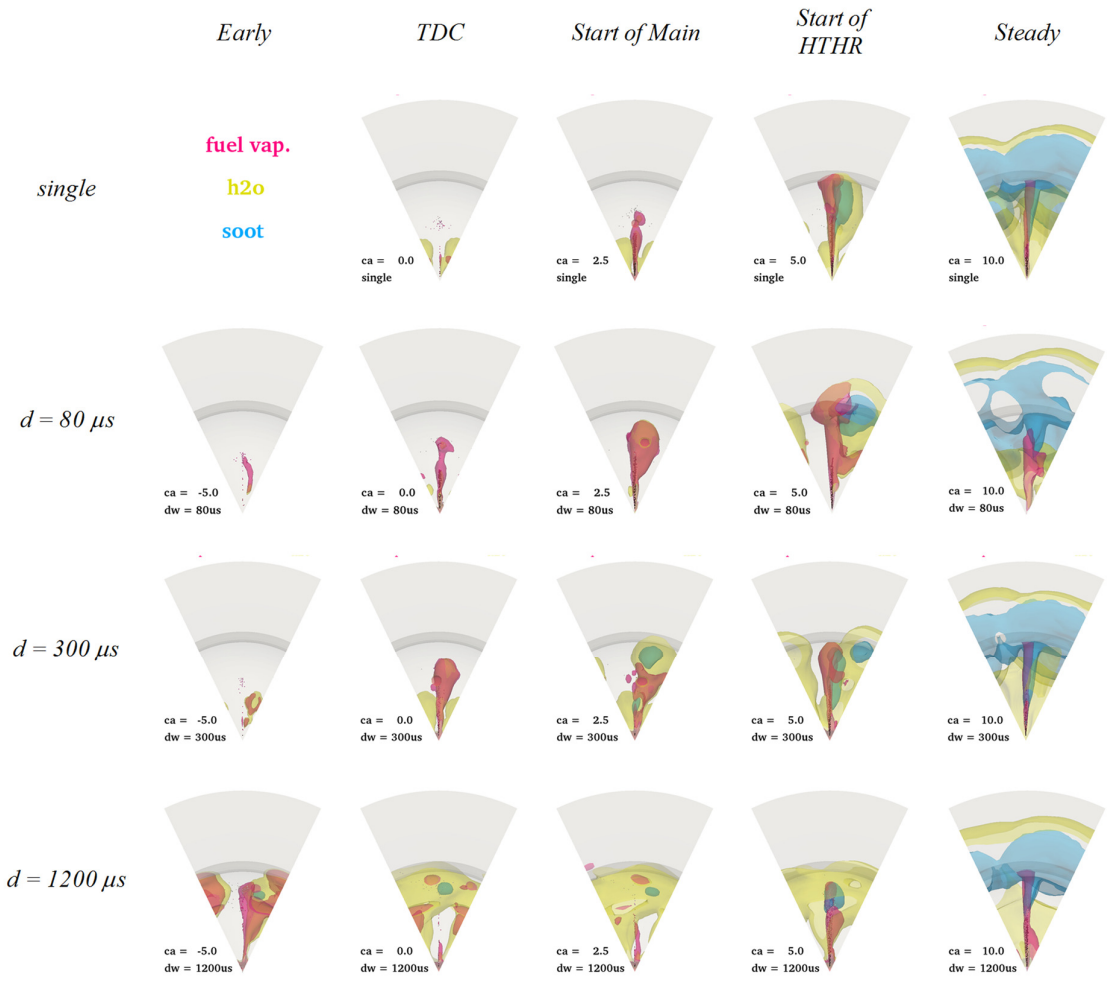

Fig. 20. Predicted diesel flame structure for single injection case and pilot-main strategies with dwell of 80, 300 and 1200 μs. (magenta) fuel vapor, (yellow) water, (cyan) soot contours enclose regions where each of these quantities has a non-negligible mass density.

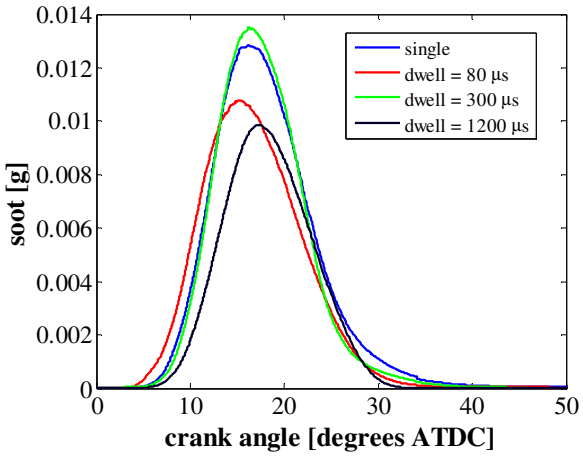

Fig. 21. Predicted in-cylinder soot for single and pilot-main strategies with dwell of 80, 300 and 1200 µs.

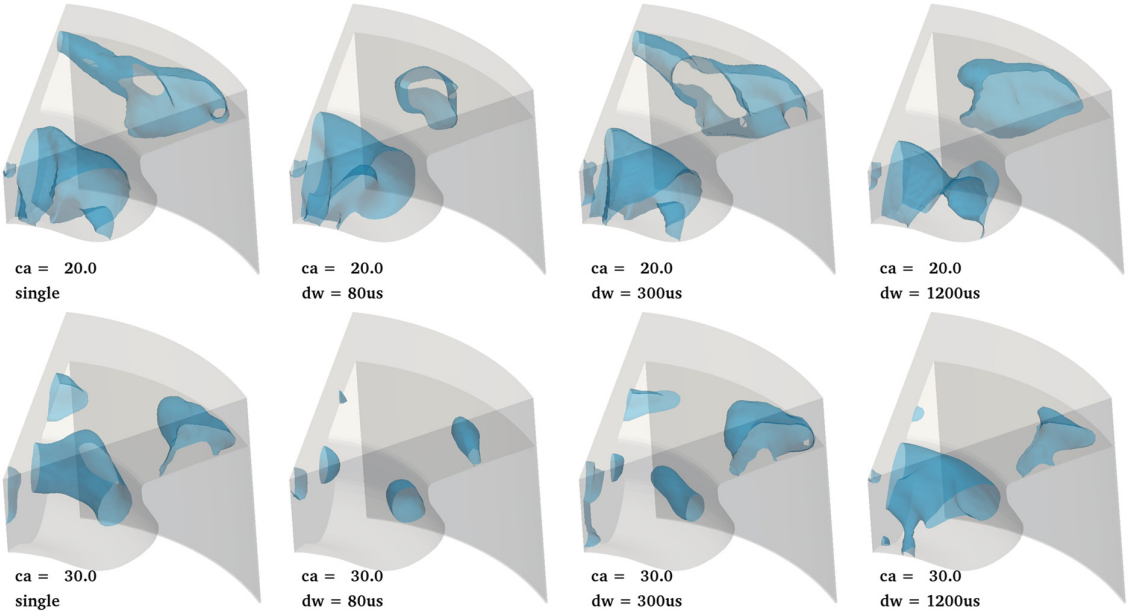

Fig. 22. Late-cycle soot cloud patterns for single and pilot-main strategies with dwell of 80, 300 and 1200 µs.

The peak pressure rise rate benefit of having a pilot injection however does not vanish completely if it is being injected too early, as also observed in [11]. With a long dwell of 1200 µs, there is enough time for the pilot to burn completely, and to mix with the surrounding charge by start of main. Figure 20 shows that that the burnt pilot-air charge does not reach the squish region, but mixes in the bowl only. The main injection is hence injected into a high-temperature environment, which however has limited reactivity because of the burnt gases; the reactive charge is reached as soon as the pilot injection splits at the bowl rim. The overall pressure rise rate is significantly smoothed, and a peak pressure rise rate similar to a dwell of 300 µs is seen, similar to what was seen in the experimental investigation of [11]. Further understanding the role of in-cylinder swirl as pilot-main dwell changes will be useful to understand how differences in the local conditions at the start of HTHR are related to swirl and the time the pilot combustion products are allowed to mix.

Soot formation.

Predicted soot formation is reported in Figure 20 in terms of a cyan sooty region, enclosing the volume where any non-negligible soot mass density is found. Global in-cylinder soot mass is reported in Figure

21. The soot formation mechanism appears strongly linked to the instantaneous flame structure behavior. In particular, late during the main pulse (e.g., at 10 degrees aTDC), when the initial mixture distribution created by the pilot injection has been destroyed by the strong injection momentum, all cases exhibit a similar soot formation structure. Soot forms in the inner jet core where the oxygen availability is limited by a maximum fuel vapor concentration, and is then transported against the rim, where it is split between the squish region and the deeper bowl region.

The soot oxidation process is governed by the bowl flow. As seen in the predicted late-cycle soot structures (Figure 22), the soot advected to the squish region oxidizes effectively, while the soot cloud in the bowl still retains its bulk structure even at 30 degrees aTDC. The figure suggests that the complex sooty structure in the bowl reduces to a close-to-toroidal region surrounding the bowl rim, both for the single injection and for most pilot dwell timings. This seems to suggest that this region is being enclosed by the tumbling vortex created by the lower half of the jet as it impacts against the rim and travels all the way along the piston bowl surface. The reason for slow soot oxidation in this region may hence be caused by the tumbling flow pattern, limiting mixing and oxygen availability in this region. However, in the real engine geometry some factors – such as valve cutouts on the piston surface – might break the azimuthal symmetry of this tumbling vortex. Hence, a more quantitative analysis of this effect using a full-engine model is needed.

Conclusions

In this work computational modeling of the effects of pilot injection dwells on combustion noise and soot emissions in a light-duty diesel engine was performed. Thorough model assessment and validation was performed against reference experimental measurements of reacting and non-reacting fuel spray development in the Engine Combustion Network constant-volume chamber, as well as against local in-cylinder mixture formation PLIF measurements in the same optically-accessible light-duty engine. The pilot injection study in the engine considered a main CDC injection pulse, preceded by a pilot injection, displaced 80 to 1200 μs earlier than the main injection event. From the analysis of in-cylinder soot distributions and pressure traces, the following concluding remarks could be drawn:

- Combustion noise benefits from adding a pilot injection provided it is not too close to the main injection. In the latter case, a unique premixed burn event is formed, causing a significantly higher peak pressure rise rate. In-cylinder analysis suggested that this phenomenon happens when the dwell is just enough to allow the pilot injection to penetrate up to the bowl rim by the start of main injection;
- The computational study confirmed the experimental finding of [11] that large dwells are as effective as smaller ones in reducing peak pressure rise rate. Regardless of the dwell time, the mechanism of noise reduction appears to be correlated with the creation of a well-mixed *burnt* region azimuthally surrounding the spray plume up to bowl rim. This region reduces the amount of premixed burn by diluting the charge from the main injection and increasing its temperature;
- Soot formation is noticeably correlated with the same mechanism. If the pilot injection is far enough from the main, it does not produce relevant amounts of soot. Hence, most soot formation is due to the main injection pulse alone, or to the main injection pulse partially overlapping with the pilot mixture when it is too close to the main (e.g., 80 μs dwell). Similarly, the soot oxidation process appears to be more correlated with the late-cycle tumbling flow structure than with the pilot-main strategy. A near-toroidal sooty structure remains until late in the cycle due to mixing being limited by the tumbling vortex generated by the lower half of the main's jet. Further understanding will require a complete engine model, flow and geometry non-uniformities.

Acknowledgements

This work was performed at the University of Wisconsin-Madison Engine Research Center and at the Combustion Research Facility of Sandia National Laboratories in Livermore, California. Support for this research was provided by the U.S. Department of Energy, Office of Vehicle Technologies, program managers Leo Breton, Gupreet Singh. Sandia is a multi-program laboratory operated by Sandia Corporation, a Lockheed Martin Company, for the United States Department of Energy's National Nuclear Security Administration under contract DE-AC04-94AL85000.

The authors would also like to acknowledge ANSYS inc. for granting ICEM CFD licenses for mesh generation to the Engine Research Center.

Nomenclature

AHRR	Apparent Heat Release Rate [J/deg CA]
BDC	Bottom Dead Center
CA	Crank Angle
CFD	Computational Fluid Dynamics
CDC	Conventional Diesel Combustion
CN	Cetane Number
DPRF	Diesel Primary Reference Fuel (binary mixture of iso-cetane and n-hexadecane)
ECN	Engine Combustion Network
EGR	Exhaust Gas Recirculation
FRESCO	Fast, Robust Engine Simulation Code
GRNG	Generalized Re-Normalization Group
IMEPg	Gross Indicated Mean Effective Pressure
KH-RT	Kelvin-Helmholtz, Rayleigh-Taylor
NSC	Nagle and Strickland-Constable's soot oxidation model
PLIF	Planar Laser-Induced Fluorescence
PPC	Partially-Premixed Combustion
PRF	Primary Reference Fuel (binary mixture of iso-octane and n-heptane)
RNG	Re-Normalization Group
ROI	Region of Interest
SNL	Sandia National Laboratories
TDC	Top Dead Center

References

1. Russell, M., Young, C., and Nicol, S., "Modulation of Injection Rate to Improve Direct Injection Diesel Engine Noise," SAE Technical Paper 900349, 1990, doi:10.4271/900349.
2. Dürnholz, M., Endres, H., and Frisse, P., "Preinjection A Measure to Optimize the Emission Behavior of DI-Diesel Engine," SAE Technical Paper 940674, 1994, doi:10.4271/940674.
3. The new 1.3 Multijet II 95 HP (Euro5) engine is making its first appearance on the Fiat 500 and 500C. Fiat Group Automobile Press, 25 Nov. 2009. <www.fiatgroupautomobilespress.com/cartelle/zoom/4594>, Available March 2016.
4. Diesel Systems: Common Rail Systems CRS2 with 1,600 to 2,000 bar and solenoid injectors. Robert Bosch GmbH, Diesel Systems, 2011. Available online March 2016.
5. Badami, M., Millo, F., and D'Amato, D., "Experimental Investigation on Soot and NOx Formation in a DI Common Rail Diesel Engine with Pilot Injection," SAE Technical Paper 2001-01-0657, 2001, doi:10.4271/2001-01-0657.
6. Ricaud, J.C. and Lavoisier, F., "Optimizing the multiple injection settings on an HSDI diesel engine," Proceedings of the Conference on Thermo- and Fluid-Dynamic Processes in Diesel Engines, THIESEL, pp. 251-275, Valencia, 2002.
7. Sahoo, D., Miles, P., Trost, J., and Leipertz, A., "The Impact of Fuel Mass, Injection Pressure, Ambient Temperature, and Swirl Ratio on the Mixture Preparation of a Pilot Injection," SAE Int. J. Engines 6(3):1716-1730, 2013, doi:10.4271/2013-24-0061.
8. Miles, P., Sahoo, D., Busch, S., Trost, J. et al., "Pilot Injection Ignition Properties Under Low-Temperature, Dilute In-Cylinder Conditions," SAE Int. J. Engines 6(4):1888-1907, 2013, doi:10.4271/2013-01-2531.
9. F. Perini, D. Sahoo, P.C. Miles, R.D. Reitz, "Modeling the Ignitability of a Pilot Injection for a Diesel Primary Reference Fuel: Impact of Injection Pressure, Ambient Temperature and Fuel Mass" , SAE Int. J. Fuels Lubr. April 2014(7):48-64; doi:10.4271/2014-01-1258.
10. Busch, S., Zha, K., Miles, P.C., "Investigations of closely coupled pilot and main injections as a means to reduce combustion noise in a small-bore direct injection Diesel engine", International Journal of Engine Research 16(1), 13-22, 2015. Doi:10.1177/1468087414560776.

11. Busch, S., Zha, K., Miles, P., Warey, A. et al., "Experimental and Numerical Investigations of Close-Coupled Pilot Injections to Reduce Combustion Noise in a Small-Bore Diesel Engine," SAE Int. J. Engines 8(2):2015, doi:10.4271/2015-01-0796.
12. Busch, S., Zha, K., Warey, A., Pesce, F., Peterson, R., "On the Reduction of Combustion Noise by a Close-Coupled Pilot Injection in a Small-Bore Direct-Injection Diesel Engine", ASME J. Eng. Gas Turbines Power 138(10), 102804, 2016.
13. Busch, S., Park, C., Warey, A., Peterson, R., Pesce, F.C., "A Study of the Impact of Pilot-Main Dwell on Late-Cycle Flow in the Piston Bowl of a Light-Duty Optical Diesel Engine", 12th International Symposium on Combustion Diagnostics, Baden-Baden, 2016.
14. Perini, F., Reitz, R.D., "Introducing FRESCO: a fast, reliable engine simulation code", DOE AEC/HCCI Program Review Meeting, Southfield, MI, August 18-20, 2015.
15. Dempsey, A. B., Wang, B. L., Reitz, R. D., Miles, P. C., Petersen, B. P., Dipankar, S., "Comparison of Quantitative In-Cylinder Equivalence Ratio Measurements with CFD Predictions for a Light Duty Low Temperature Combustion Diesel Engine", SAE Technical paper 2012-01-0143, 2012.
16. F. Perini, A.B. Dempsey, R.D. Reitz, D. Sahoo, B. Petersen, P.C. Miles, "A Computational Investigation of the Effects of Swirl Ratio and Injection Pressure on Mixture Preparation and Wall Heat Transfer in a Light-Duty Diesel Engine", SAE Technical paper 2013-01-1105, SAE 2013 World Congress & Exhibition 2013, Detroit, MI, 2013.
17. F. Perini and R.D. Reitz, "Improved atomization, collision and sub-grid scale momentum coupling models for transient vaporizing engine sprays", International Journal of Multiphase Flows 79(2016), 107-123. doi:10.1016/j.ijmultiphaseflow.2015.10.009.
18. F. Perini, E. Galligani, R.D. Reitz, "A study of direct and Krylov iterative solver techniques to approach linear scaling of the integration of Chemical Kinetics with detailed combustion mechanims", Combustion and Flame 161(5), 1180-1195, 2014.
19. F. Perini, "High-dimensional, unsupervised cell clustering for computationally efficient engine simulations with detailed combustion chemistry", Fuel 106, 344-356, 2012.
20. Wang, B.-L., Lee, C.-W., Reitz, R.D., Miles, P.C., and Han, Z., "A Generalized RNG turbulence model and its application to a light-duty diesel engine operating in a low temperature combustion regime," International Journal of Engine Research, Vol. 14, Issue 3, pp. 279-292, 2013.
21. Beale, J. C. Beale and Reitz, R. D. Reitz, "Modeling Spray Atomization with the Kelvin-Helmholtz/Rayleigh-Taylor hybrid model," Atomization and Sprays, 1999, Volume 9, pp. 623-650.
22. R.D. Reitz, F.V. Bracco, "On the Dependence of the Spray Angle and Other Spray Parameters on Nozzle Design and Operating Conditions," SAE Technical paper 790494 , 1979.
23. Munnannur, A., Reitz, R.D., "Comprehensive collision model for multidimensional engine spray computations", Atomization and Sprays 19(7), 597-619, 2009. doi:10.1615/AtomizSpr.v19.i7.10.
24. Torres, D.J., O'Rourke, P.J., Amsden, A.A., "A discrete multicomponent fuel model", Atomization and Sprays 13(2-3), 42 pages, 2003. Doi:10.1615/AtomizSpr.v13.i23.10.
25. Pickett L.M., Manin J., Genzale C.L., Siebers D.L., Musculus M.P.B., Idicheria C.A. (2011) "Relationship between diesel fuel spray vapor penetration/dispersion and local fuel mixture fraction," SAE Int. J. Engines 4(1):764-799 doi:10.4271/2011-01-0686.
26. Lillo, P.M., Pickett, L.M., Kook, S., Persson, H., and Andersson, Ö. (2012) "Diesel Spray Ignition Detection and Spatial/Temporal Correction," SAE Technical Paper 2012-01-1239.
27. Wang, H., Ra, Y., Jia, M., and Reitz, R.D., "Development of a Reduced n-dodecane-PAH Mechanism and its Application for n-dodecane Soot Predictions," Fuel 136, 25-36, 2014, http://dx.doi.org/10.1016/j.fuel.2014.07.028.
28. Hessel, R., Reitz, R., Musculus, M., O'Connor, J. et al., "A CFD Study of Post Injection Influences on Soot Formation and Oxidation under Diesel-Like Operating Conditions," SAE Int. J. Engines 7(2):2014, doi:10.4271/2014-01-1256.
29. Nishida, K. and Hiroyasu, H., "Simplified Three-Dimensional Modeling of Mixture Formation and Combustion in a D.I. Diesel Engine," SAE Technical Paper 890269, 1989, doi:10.4271/890269.
30. Nagle, J., Strickland-Constable, R. F., "Oxidation of Carbon between 1000-2000 C," Proc. of the Fifth Carbon Conf 1, p. 154, 1962.
31. Vishwanathan, G., Reitz, R.D., "Application of a semi-detailed soot modeling approach for conventional and low temperature diesel combustion - Part I: Model Performance," Fuel, Vol. 139(1), pp. 757-770, 2015. http://dx.doi.org/10.1016/j.fuel.2014.08.026, 2014
32. Skeen, S.A., Engine Combustion Network 2.3, http://www.sandia.gov/ecn/workshop/ECN2.3.mp4, Accessed May 2016.
33. Skeen, S., Manin, J., Pickett, L., Cenker, E. et al., "A Progress Review on Soot Experiments and Modeling in the Engine Combustion Network (ECN)," SAE Int. J. Engines 9(2):2016, doi:10.4271/2016-01-0734.

34. Dec, J., "A Conceptual Model of DI Diesel Combustion Based on Laser-Sheet Imaging*," SAE Technical Paper 970873, 1997, doi:10.4271/970873.
35. Skeen, S.A., Manin, J., Dalen, K., Pickett, L.M., “Extinction-based Imaging of Soot Processes over a Range of Diesel Operating Conditions”, 8th U.S. National Combustion Meeting, Salt Lake City, UT, 2013.
36. Aizawa, T., Nishigai, H., Kondo, K., Yamaguchi, T., Nerva, J., Genzale, C., Kook, S., Pickett, L., “Transmission Electron Microscopy of Soot Particles Directly Sampled in Diesel Spray Flame – A Comparison between US#2 and Biodiesel Soot”, SAE Int. J. Fuels Lubr. 5(2):665-673, 2012, doi:10.4271/2012-01-0695.
37. Pope, S.B., “An Explanation of the turbulent round-jet/plane-jet anomaly”, AIAA Journal, vol. 16 No. 3 (1978), pp. 279-281.